Summer 5-2011

Analysis of a monolithic crystal plate acoustic wave filter

Huijing He
University of Nebraska-Lincoln, he.hui.jing@hotmail.com

Ultrasonics 51 (2011) 991–996

Contents lists available at ScienceDirect

Ultrasonics

journal homepage: www.elsevier.com/locate/ultras

Analysis of a monolithic crystal plate acoustic wave filter

Huijing He [a], Jinxi Liu [a,*], Jiashi Yang [b]

[a] Department of Engineering Mechanics, Shijiazhuang Tiedao University, Shijiazhuang 050043, China
[b] Department of Engineering Mechanics, University of Nebraska, Lincoln, NE 68588-0526, USA

ARTICLE INFO

Article history:
Received 22 April 2011
Accepted 25 May 2011
Available online 7 June 2011

Keywords:
Quartz
Crystal
Plate
Thickness–shear vibration
Thickness–twist vibration

ABSTRACT

We study thickness–shear and thickness–twist vibrations of a finite, monolithic, AT-cut quartz plate crystal filter with two pairs of electrodes. The equations of anisotropic elasticity are used with the omission of the small elastic constant c_{56}. An analytical solution is obtained using Fourier series from which the resonant frequencies, mode shapes, and the vibration confinement due to the electrode inertia are calculated and examined.

1. Introduction

Piezoelectric crystals are widely used to make acoustic wave resonators, filters and sensors for time-keeping, frequency generation and operation, telecommunication, and sensing. Quartz is the most widely used crystal for these applications. A large portion of quartz crystal devices operate with thickness–shear (TSh) vibration modes of a plate [1,2]. Theoretically, TSh modes can only exist in unbounded plates without edge effects. When a plate is vibrating in TSh modes, motions of material particles are parallel to the surfaces of the plate, and particle velocities vary along the plate thickness only, without in-plane variations. TSh modes are the ideal operating modes of many acoustic wave devices.

In reality, however, due to the finite sizes of devices, pure TSh modes cannot exist in finite crystal plates because of edge effects. Therefore, in real devices, the actual operating modes have slow, in-plane variations. These real modes have been referred to as transversely varying TSh modes [3]. Another cause of in-plane variations of TSh modes is when a crystal plate is partially electroded in the central region [4], a common situation of crystal resonators. In such a case the inertia of the electrodes is responsible for an important phenomenon called energy trapping through which the vibration is confined under the electrodes and decays rapidly outside them. Energy trapping is crucial to device mounting. When energy trapping exists, plates can be mounted near the edges where there is no vibration and therefore the operation of the device is not affected by mounting.

Because of the complications associated with the material anisotropy of quartz, analysis of TSh modes with in-plane variations usually presents considerable mathematical challenges. In most cases approximate two-dimensional (2D) plate equations [5–7] which are much simpler than the three-dimensional equations of elasticity or piezoelectricity are used. There exist systematic theoretical results from the 2D plate equations for TSh modes with in-plane variation in one direction only, i.e., in the direction parallel to the TSh particle velocity. Free vibration modes of finite plates with free edges and their frequency spectra [8–10], energy trapping in partially electroded plates and Bechmann's number regarding electrode dimension [4], monolithic filters with two pairs of electrodes [11], arrays of multiple resonators [12,13], and resonator capacitance from forced vibration analyses [14] have been obtained.

In the case when the in-plane mode variation is in the direction perpendicular to the TSh particle velocity, the corresponding waves are called thickness–twist (TT) waves [15,16]. For this case reported studies are much fewer. Propagating waves in unbounded plates with or without electrodes were studied in [15–18], with an expression of Bechmann's number given in [16]. Since crystal devices are made smaller and smaller for miniaturization, edge effects become more pronounced and in-plane variations in both directions are equally important. It is our recent effort to provide new understandings of TT waves to reach the same level as the knowledge of the in-plane variation in the other direction.

In this paper we study TT modes in an AT-cut quartz plate partially covered by two pairs of electrodes as a crystal filter. We use the equations of anisotropic elasticity instead of the 2D plate equations. The only approximation made is the omission of the small elastic constant c_{56} which is a common approximation in the anal-

* Corresponding author.
E-mail address: liujx02@hotmail.com (J. Liu).

0041-624X/$ - see front matter © 2011 Elsevier B.V. All rights reserved.
doi:10.1016/j.ultras.2011.05.015

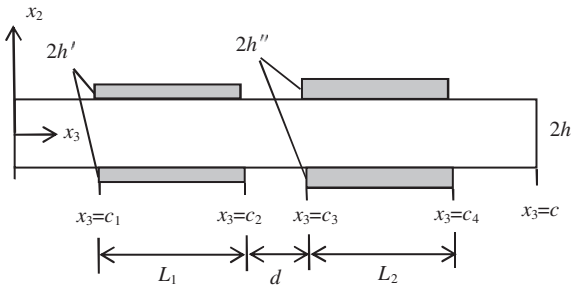

Fig. 1. An AT-cut quartz plate with two pairs of electrodes as a monolithic filter.

ysis of quartz plates. We want to examine how the resonant frequencies, mode shapes, and energy trapping are affected by the electrode mass, dimension, and position.

2. Governing equations

The equations for anisotropic crystals vary considerably according to crystal symmetry. A particular cut of a crystal plate refers to the orientation of the plate when it is taken out of a bulk crystal. As a consequence crystal plates of different cuts exhibit different material anisotropies in coordinates normal and parallel to the plate surfaces. The widely used AT-cut quartz plate is a special case of rotated Y-cut quartz plates which are effectively monoclinic in

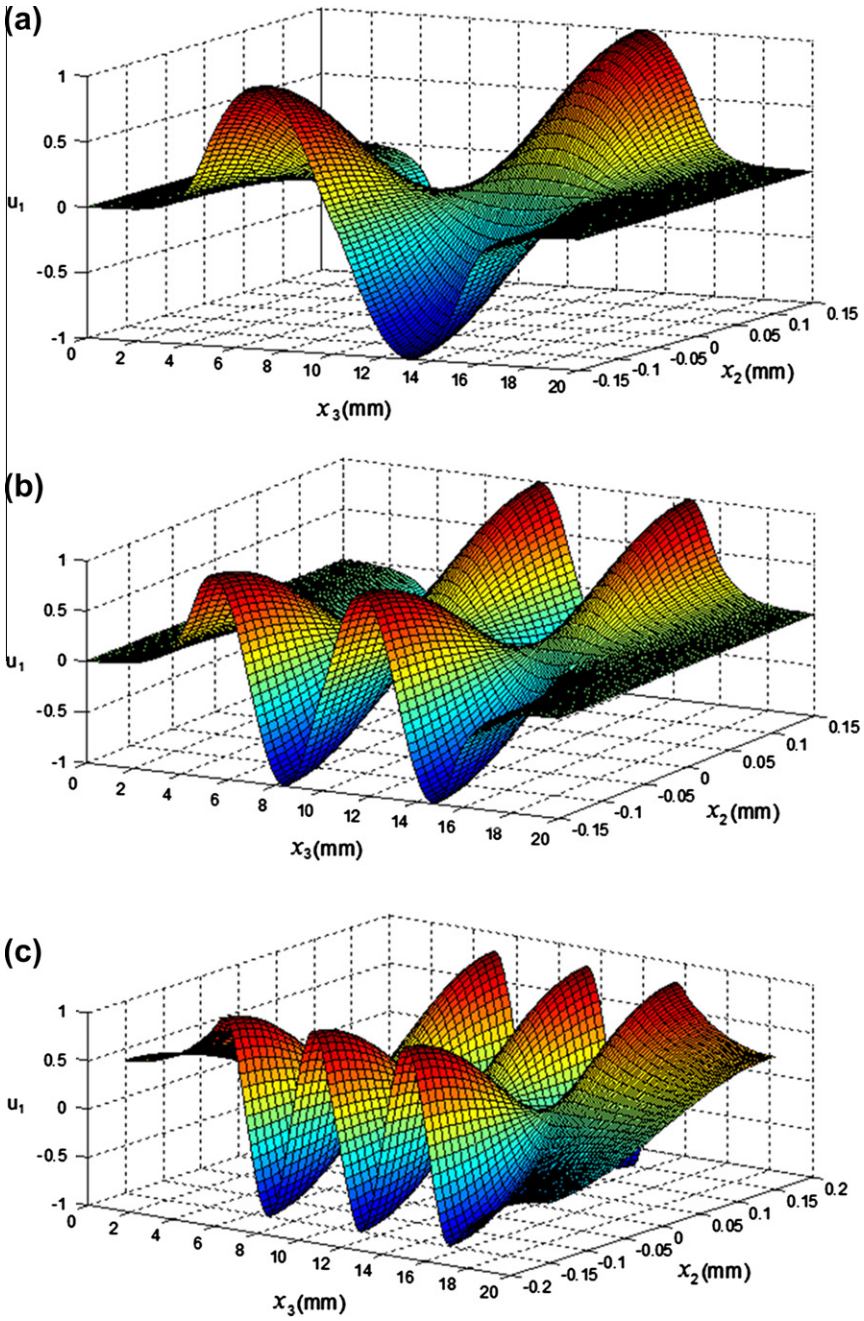

Fig. 2. Antisymmetric trapped modes (identical electrodes).

the plate coordinate system. Consider such a plate as shown in Fig. 1. The plate is unbounded in the x_1 direction and does not vary along x_1. Fig. 1 shows a cross section. It carries two pairs of electrodes (left pair and right pair) at the top and bottom surfaces, symmetric about the middle plane of the plate. The electrodes are assumed to be very thin. Their inertia will be considered but their stiffness will be neglected. Quartz has very weak piezoelectric coupling. For free vibration frequency analysis the small piezoelectric coupling can usually be neglected and an elastic analysis is sufficient. For monoclinic crystals, shear-horizontal or antiplane motions with only one displacement component are allowed by the linear theory of anisotropic elasticity. The corresponding modes are TT modes in general and include TSh and face-shear modes as special cases. Shear-horizontal motions in rotated Y-cut quartz are described by:

$$u_1 = u_1(x_2, x_3, t), \quad u_2 = u_3 = 0, \tag{1}$$

where **u** is the displacement vector. The nonzero components of the strain tensor **S** and the stress tensor **T** are:

$$S_5 = 2S_{31} = u_{1,3}, \quad S_6 = 2S_{21} = u_{1,2}, \tag{2}$$

$$T_{31} = c_{55}u_{1,3} + c_{56}u_{1,2}, \quad T_{21} = c_{56}u_{1,3} + c_{66}u_{1,2}, \tag{3}$$

where **c** is the elastic stiffness tensor. The relevant equation of motion is

$$T_{21,2} + T_{31,3} = \rho\ddot{u}_1. \tag{4}$$

The equation to be satisfied by u_1 is obtained by substituting (3) into (4):

$$c_{66}u_{1,22} + c_{55}u_{1,33} + 2c_{56}u_{1,23} = \rho\ddot{u}_1. \tag{5}$$

For the plate in Fig. 1, the boundary conditions at the plate top and bottom are:

$$T_{21} = \begin{cases} \mp 2\rho' h'\ddot{u}_1, & x_2 = \pm h, \ c_1 < x_3 < c_2, \\ \mp 2\rho' h''\ddot{u}_1, & x_2 = \pm h, \ c_3 < x_3 < c_4, \\ 0, & x_2 = \pm h, \ 0 < x_3 < c_1, \ c_2 < x_3 < c_3, \quad \text{or } c_4 < x_3 < c, \end{cases} \tag{6}$$

where ρ' is the density of the electrodes. $2h'$ and $2h''$ are their thickness. In the electroded areas of the plate surfaces, the boundary conditions in (6) represent Newton's second law applied to the electrodes. The boundary conditions at the left and right edges are

$$T_{31} = 0, \quad x_3 = 0, \quad c, \quad |x_2| < h. \tag{7}$$

For AT-cut quartz plates, $c_{55} = 68.81$, $c_{56} = 2.53$ and $c_{66} = 29.01 \times 10^9$ N/m^2 [11]. c_{56} is very small compared to c_{55} and c_{66}. Therefore, in the rest of this paper, we will make the usual approximation of neglecting the small c_{56} [19].

3. Fourier series solution

Consider free vibrations. Let

$$u_1(x_2, x_3, t) = u_1(x_2, x_3)\exp(i\omega t). \tag{8}$$

The plate in Fig. 1 is symmetric about its middle plane. For the applications we are considering, we are interested in motions antisymmetric in x_2. Therefore we construct the following solution from separation of variables:

$$u_1 = B_0 \sin(\eta_0 x_3) + \sum_{m=1}^{\infty} B_m \sin(\eta_m x_2)\cos\frac{m\pi x_3}{c}, \tag{9}$$

where B_0 and B_m are undetermined constants, and

$$\eta_m^2 = \frac{\rho\omega^2}{c_{66}} - \frac{c_{55}}{c_{66}}\left(\frac{m\pi}{c}\right)^2 = \frac{\pi^2}{4h^2}\left[\frac{\omega^2}{\omega_s^2} - \frac{c_{55}}{c_{66}}\left(m\frac{2h}{c}\right)^2\right], \quad m = 0, 1, 2, 3, \ldots, \tag{10}$$

$$\omega_s = \frac{\pi}{2h}\sqrt{\frac{c_{66}}{\rho}}. \tag{11}$$

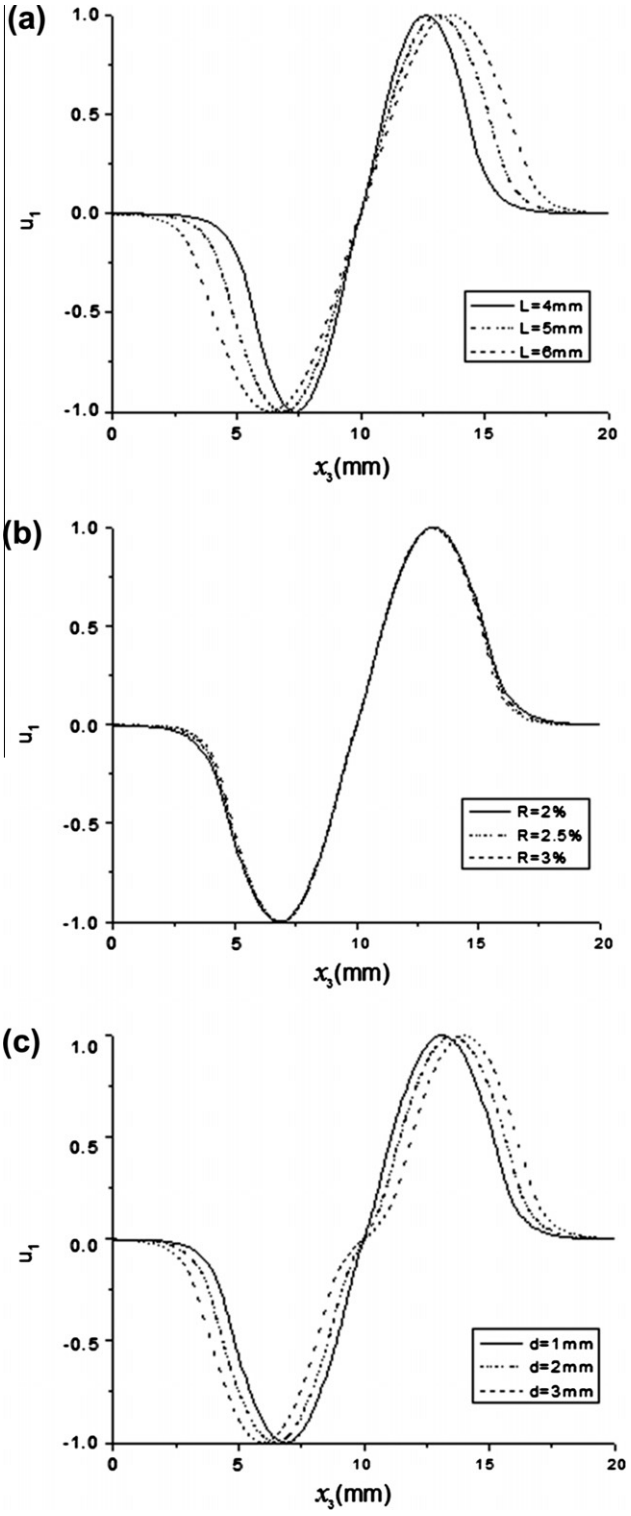

Fig. 3. Effects of electrode parameters on antisymmetric modes (identical electrodes).

(9) satisfies (5) and (7) when the small c_{56} is neglected. ω_s is the resonant frequency of the fundamental thickness–shear mode in an unbounded quartz plate. Quartz resonators are usually with large length/thickness ratios, i.e., $c \gg 2h$. In this case, for an m that is not large, η_m^2 is positive. We are interested in the first few TSh and TT modes with no more than a few nodal points along the x_3 direction for which a large m is not needed. In the case when a large m is indeed needed, we can redefine η_m^2 with a minus sign and change the sine functions in (9) into hyperbolic sine functions. In the following we will formally use (9) and (10) and implement the changes for large m in the computer code when needed. To apply the boundary conditions at the plate top and bottom, we need

$$T_{21} = c_{66}u_{1,2} = c_{66}B_0\eta_0\cos(\eta_0 x_3) + c_{66}\sum_{m=1}^{\infty} B_m\eta_m\cos(\eta_m x_2)\cos\frac{m\pi x_3}{c}. \quad (12)$$

Due to the antisymmetry of the modes about the plate middle plane, the boundary conditions at $x_2 = -h$ do not provide equations independent to the boundary conditions at $x_2 = h$. Substitution of (9) and (12) into to the boundary conditions at $x_2 = h$ in (6) gives

$$c_{66}B_0\eta_0\cos(\eta_0 h) + c_{66}\sum_{m=1}^{\infty} B_m\eta_m\cos(\eta_m h)\cos\tfrac{m\pi x_3}{c} = \begin{cases} 2\rho' h'\omega^2[B_0\sin(\eta_0 h) + \sum_{m=1}^{\infty} B_m\sin(\eta_m h)\cos\tfrac{m\pi x_3}{c}], & c_1 < x_3 < c_2, \\ 2\rho' h''\omega^2[B_0\sin(\eta_0 h) + \sum_{m=1}^{\infty} B_m\sin(\eta_m h)\cos\tfrac{m\pi x_3}{c}], & c_3 < x_3 < c_4, \\ 0, \quad 0 < x_3 < c_1,\ c_2 < x_3 < c_3,\ \text{or}\ c_4 < x_3 < c. \end{cases} \quad (13)$$

We multiply both sides of (13) by $(n\pi x_3/c)$ $(n = 0, 1, 2, \ldots)$ and integrate the resulting expression over $(0, c)$ to obtain

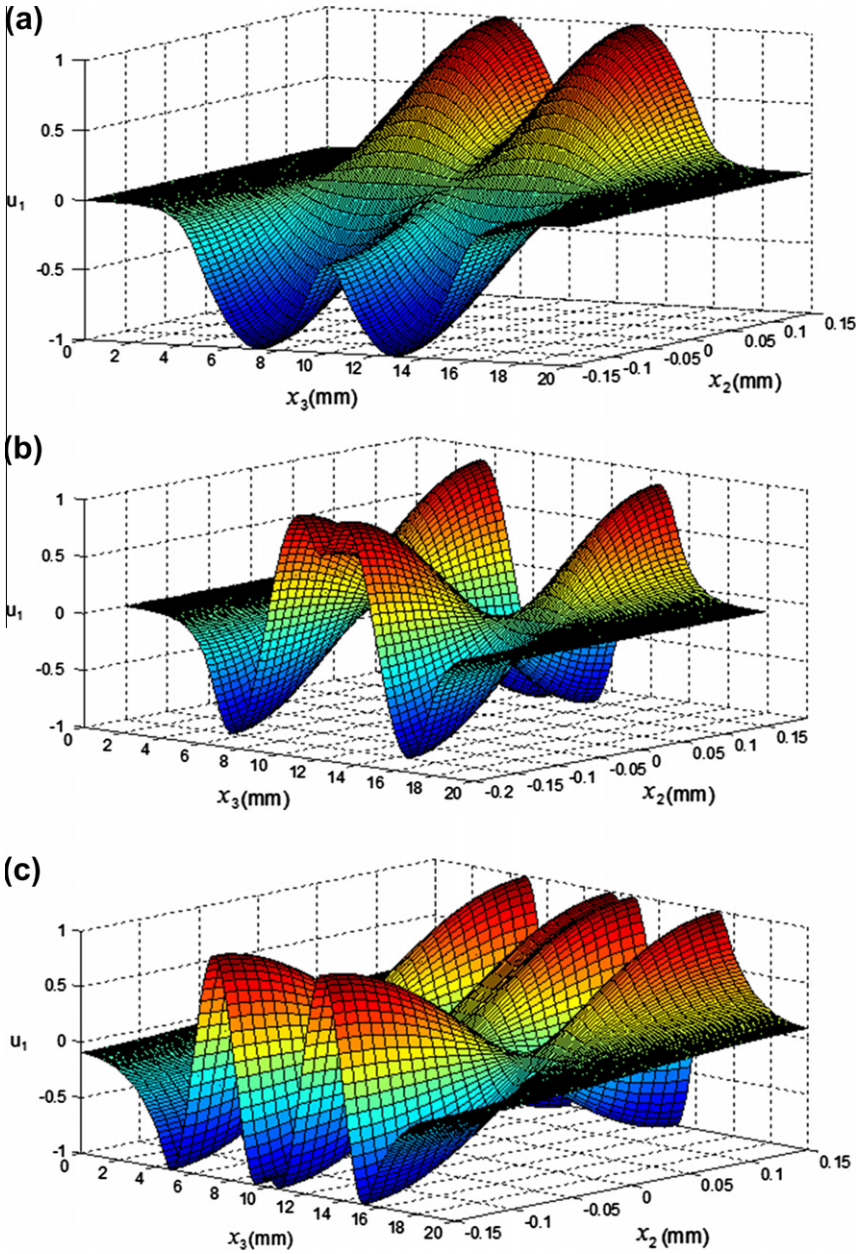

Fig. 4. Symmetric trapped modes (identical electrodes).

$$c_{66}B_0\eta_0\cos(\eta_0 h)c = 2\rho' h'\omega^2 B_0\sin(\eta_0 h)(c_2-c_1) + 2\rho' h'\omega^2\sum_{m=1}^{\infty}B_m\sin(\eta_m h)\frac{c}{m\pi}\left(\sin\frac{m\pi c_2}{c}-\sin\frac{m\pi c_1}{c}\right) + 2\rho' h''\omega^2 B_0\sin(\eta_0 h)(c_4-c_3) + 2\rho' h''\omega^2\sum_{m=1}^{\infty}B_m\sin(\eta_m h)\frac{c}{m\pi} \times\left(\sin\frac{m\pi c_4}{c}-\sin\frac{m\pi c_3}{c}\right),\quad n=0, \tag{14}$$

and

$$\frac{c}{2}c_{66}B_n\eta_n\cos(\eta_n h) = 2\rho' h'\omega^2 B_0\sin(\eta_0 h)\frac{c}{n\pi}\left(\sin\frac{n\pi c_2}{c}-\sin\frac{n\pi c_1}{c}\right) + 2\rho' h'\omega^2\sum_{m=1}^{\infty}B_m\sin(\eta_m h)C_{nm} + 2\rho' h''\omega^2 B_0\sin(\eta_0 h)\frac{c}{n\pi}\left(\sin\frac{n\pi c_4}{c}-\sin\frac{n\pi c_3}{c}\right) + 2\rho' h''\omega^2\sum_{m=1}^{\infty}B_m\sin(\eta_m h)D_{nm},\quad n=1,2,3,\ldots, \tag{15}$$

where

$$C_{nm}=\int_{c_1}^{c_2}\cos\tfrac{n\pi x_3}{c}\cos\tfrac{m\pi x_3}{c}dx_3=C_{mn},\qquad D_{nm}=\int_{c_3}^{c_4}\cos\tfrac{n\pi x_3}{c}\cos\tfrac{m\pi x_3}{c}dx_3=D_{mn},\quad n=1,2,3,\ldots. \tag{16}$$

(14) and (15) are linear homogeneous equations for B_0 and B_m. For nontrivial solutions the determinant of the coefficient matrix has to vanish, which determines the resonant frequencies. The nontrivial solutions of B_0 and B_m determine the corresponding modes. This is a complicated eigenvalue problem because the eigenvalue or the resonant frequency is present in every η_m.

4. Numerical results

As an example we first consider a filter of AT-cut quartz with four identical electrodes. $L_1 = L_2 = L = 5$ mm and $R_1 = R_2 = R = 2.5\%$, where $R_1 = \rho' h'/(\rho h)$ and $R_2 = \rho' h''/(\rho h)$. The distance between the two pairs of electrodes is $d = 1$ mm. The geometric parameters are $c = 20$ mm, $c_1 = 4.5$ mm, $c_2 = 9.5$ mm, $c_3 = 10.5$ mm, $c_4 = 15.5$ mm, and $2h = 0.3$ mm. The material constants needed can be found in [11]. The structure is symmetric about $x_3 = c/2$. Accordingly modes can be separated into symmetric ones and antisymmetric ones about $x_3 = c/2$. $\omega_s = 3.46546489\times10^7$ rad/s. The frequencies of the modes we are interested in are within $\omega_s(1-R)<\omega<\omega_s$.

Three modes antisymmetric about $x_3 = c/2$ are found and are shown in Fig. 2 in the order of increasing frequency. $\omega_1 = 3.39064675\times10^7$ rad/s, $\omega_2 = 3.41890214\times10^7$ rad/s, and $\omega_3 = 3.46086051\times10^7$ rad/s. The modes have slow variations in the x_3 direction, with no more than a few nodal points (zeros). Numerical tests show that to describe such a slow variation we do not need many terms in the series. When using 20 terms in the series, $\omega_1 = 3.39064675\times10^7$ rad/s. When using 19 terms, $\omega_1 = 3.39064680\times10^7$ rad/s. There are 8 significant figures. The corresponding modes also show good agreement. Therefore all calculations below are with 20 terms in the series. In this case the η_m^2 in (10) is positive. For all of the modes in Fig. 2 the vibration is small near the plate edges at $x_3 = 0, c$. This is the so-called energy trapping phenomenon. In the first mode, there is one nodal point along the x_3 direction in the middle between the two pairs of the electrodes. The vibrations under the two pairs of electrodes are with opposite signs (out of phase). Such a mode can be driven by opposite voltages on the two pairs of electrodes. The other modes all have more nodal points. When modal points are present under the electrodes, the charges on the electrodes produced by the shear strain of the plate tend to cancel with each other. This may be undesirable or desirable depending on the specific application.

Fig. 3 shows the effects of various parameters of the electrodes on the lowest antisymmetric mode. In Fig. 3a only the electrode length is varied (L or c_1 and c_4). When $L = 4$ mm, there are two trapped modes. When $L = 5$ or 6 mm, there are three trapped modes. As the electrodes become longer, the frequency of the first mode becomes lower due to more inertia from longer electrodes. When $L = 4$, 5, and 6 mm, $\omega_1 = 3.39476548$, 3.39064675, and 3.38812666×10^7rad/s, respectively. When the electrodes become longer, the vibration distribution becomes wider. In Fig. 3b only the electrode thickness is varied. The case of $R = 2\%$ has two trapped modes. The cases of $R = 2.5\%$ and 3% have three trapped modes. As R increases, the frequency of the first mode decreases as expected: $\omega_1 = 3.40695776$, 3.39064675, and 3.37444052×10^7 rad/s, respectively. The vibration distribution is not sensitive to R. In Fig. 3c only the distance d between the two pairs of electrodes is varied. The frequency is not sensitive to d as expected: $\omega_1 = 3.39064675$, 3.39009008, and 3.38993846×10^7 rad/s, respectively. The vibration distribution is sensitive to d. When $d = 1$ mm, the solid line in the figure is smooth. When $d = 2$ and 3 mm, the dotted lines in the figure feel the presence of the distance between the electrodes.

For the same filter as in Fig. 2, there also exist three trapped modes symmetric about $x_3 = c/2$ which are shown in Fig. 4 in the order of increasing frequency. These modes can be excited by applying the same voltage on the two pairs of electrodes. $\omega_1 =$

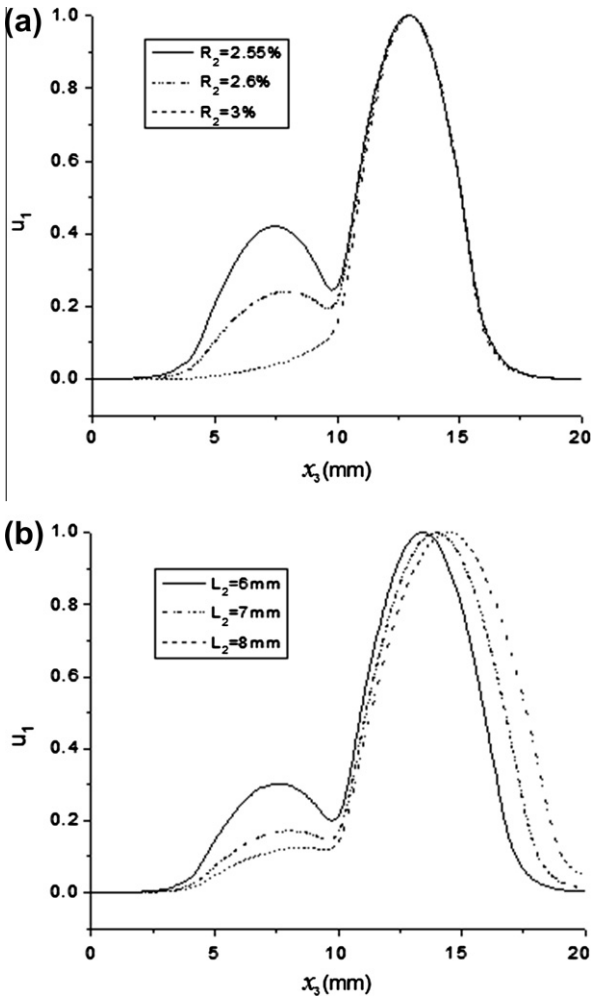

Fig. 5. Effects of electrode parameters (unequal electrodes).

3.38893137×10^7 rad/s, $\omega_2 = 3.41240560 \times 10^7$ rad/s, and $\omega_3 = 3.44943502 \times 10^7$ rad/s. These three frequencies are slightly below the frequencies of the three modes in Fig. 2. When symmetric and antisymmetric modes are considered together, the lowest mode is symmetric, followed by the first antisymmetric mode, and so on.

Fig. 5 shows the effects of electrode parameters when the thickness or length of the right pair of electrodes is varied. In this case the structure loses its symmetry about $x_3 = c/2$. For filters, even if the structure of the crystal plate and electrodes are symmetric about $x_3 = c/2$, the input and output circuits may cause loss of symmetry about $x_3 = c/2$. Therefore the examination of the effects of some small asymmetry is fundamental. In Fig. 5a R_1 is fixed to be 2.5%. R_2 is varied. When $R_2 = 2.55\%$, 2.6%, and 3%, there are always six trapped modes which can no longer be separated into symmetric and antisymmetric modes. As R_2 increases, the frequency of the first mode decreases as expected: $\omega_1 = 3.38781680$, 3.38637123, and 3.37371241×10^7 rad/s, respectively. The vibration distribution is more and more under the thicker electrodes as R_2 increases. In Fig. 5b, as the right pair of electrodes becomes longer, the frequency of the first mode becomes lower and the vibration is more and more under the longer electrodes: $\omega_1 = 3.38738566$, 3.38602462, and 3.38501809×10^7 rad/s, respectively. When $L_2 = 6$ mm, there are six trapped modes. When $L_2 = 7$ and 8 mm, there are seven trapped modes.

5. Conclusion

The Fourier series solution used is effective in the analysis of quartz crystal filters. There exist trapped modes whose frequencies are close to each other. For a symmetric structure with identical electrodes, the modes can be separated into symmetric and antisymmetric ones. The lowest mode is symmetric, followed by an antisymmetric one, and so on. The vibration distribution is sensitive to the electrode length and the distance between the two pairs of electrodes, but not sensitive to the electrode thickness. Thicker and longer electrodes lower the frequencies and increase the number of trapped modes. For unequal electrodes, modes cannot be separated into symmetric and antisymmetric ones. The vibration distribution is more under the longer or thicker electrodes.

Acknowledgments

This work is supported by the National Natural Science Foundation of China (No. 10972147) as well as the Program for Changjiang Scholars and Innovative Research Team in University (No. IRT0971).

References

[1] I. Koga, Thickness vibrations of piezoelectric oscillating crystals, Physics 3 (1932) 70–80.
[2] H.F. Tiersten, Thickness vibrations of piezoelectric plates, J. Acoust. Soc. Am. 35 (1963) 53–58.
[3] H.F. Tiersten, A corrected modal representation of thickness vibrations in quartz plates and its influence on the transversely varying case, IEEE Trans. Ultrason. Ferroelectr. Freq. Control 50 (2003) 436–1443.
[4] R.D. Mindlin, P.C.Y. Lee, Thickness–shear and flexural vibrations of partially plated crystal plates, Int. J. Solids Struct. 2 (1966) 125–139.
[5] H.F. Tiersten, R.D. Mindlin, Forced vibrations of piezoelectric crystal plates, Quart. Appl. Math. 20 (1962) 107–119.
[6] R.D. Mindlin, High frequency vibrations of piezoelectric crystal plates, Int. J. Solids Struct. 8 (7) (1972) 895–906.
[7] P.C.Y. Lee, S. Syngellakis, J.P. Hou, A two-dimensional theory for high-frequency vibrations of piezoelectric crystal plates with or without electrodes, J. Appl. Phys. 61 (4) (1987) 1249–1262.
[8] R.D. Mindlin, Thickness–shear and flexural vibrations of crystal plates, J. Appl. Phys. 22 (1951) 316–323.
[9] R.D. Mindlin, Forced thickness–shear and flexural vibrations of piezoelectric crystal plates, J. Appl. Phys. 23 (1952) 83–88.
[10] J. Wang, W.H. Zhao, The determination of the optimal length of crystal blanks in quartz crystal resonators, IEEE Trans. Ultrason. Ferroelectr. Freq. Control 52 (2005) 2023–2030.
[11] H.F. Tiersten, Linear Piezoelectric Plate Vibrations, Plenum, New York, 1969.
[12] F. Shen, K.H. Lee, S.J. O'Shea, P. Lu, T.Y. Ng, Frequency interference between two quartz crystal microbalances, IEEE Sens. J. 3 (3) (2003) 274–281.
[13] F. Shen, P. Lu, Influence of interchannel spacing on the dynamical properties of multichannel quartz crystal microbalance, IEEE Trans. Ultrason. Ferroelectr. Freq. Control 50 (6) (2003) 668–675.
[14] J. Wang, W.H. Zhao, J.K. Du, The determination of electrical parameters of quartz crystal resonators with the consideration of dissipation, Ultrasonics 44 (Suppl. 1) (2006) E869–E873.
[15] R.D. Mindlin, Thickness–twist vibrations of an infinite, monoclinic, crystal plate, Int. J. Solids Struct. 1 (1965) 141–145.
[16] R.D. Mindlin, Bechmann's number for harmonic overtones of thickness/twist vibrations of rotated Y-cut quartz plates, J. Acoust. Soc. Am. 41 (1966) 969–973.
[17] J.S. Yang, S.H. Guo, Propagation of thickness–twist waves in a quartz plate with asymmetric mass layers, IEEE Trans. Ultrason. Ferroelectr. Freq. Control 53 (2006) 1560–1561.
[18] Z.T. Yang, Y.T. Hu, J.S. Yang, Effect of mass layer stiffness on propagation of thickness–twist waves in rotated-y-cut quartz crystal plates, Ultrasonics 49 (2009) 401–403.
[19] H.F. Tiersten, Analysis of trapped-energy resonators operating in overtones of coupled thickness shear and thickness twist, J. Acoust. Soc. Am. 59 (1976) 879–888.